

Polarization-state-dependent attenuation and amplification in a columnar thin film

Tom G. Mackay¹ and Akhlesh Lakhtakia²

Abstract

We numerically investigated the plane-wave reflection–transmission characteristics of a columnar thin film (CTF) whose columns are made from a dissipative material but whose void regions are filled with an active material. By computing the reflectances and transmittances, we found that the CTF can simultaneously amplify s -polarized incident light and attenuate p -polarized incident light, or vice versa. This polarization-state-dependent attenuation and amplification phenomenon depends upon the angle of incidence and the thickness of the CTF.

Keywords: polarization state, reflection, transmission, active, dissipative, orthorhombic

The advent of nanotechnology and the emergence of metamaterials [1] has allowed composite materials with exotic optical properties to be realistically contemplated and, in some cases, actually realized. In particular, theoretical studies have revealed attractive response characteristics associated with composite materials containing both active and dissipative component materials. While active component materials have been widely incorporated into various metamaterials in an attempt to combat intrinsic losses [2–5], other applications of active component materials have cropped up more recently. For example, the homogenization of a mixture of both active and dissipative spheroidal particles engenders a uniaxial dielectric material that simultaneously exhibits both amplification and attenuation, depending upon the direction of propagation [6]. In a similar vein, interleaving layers of active and dissipative component materials leads to a birefringent material which facilitates arbitrary control over polarization states [7]. Homogenization can also lead to an isotropic chiral material that amplifies left-circularly polarized light but attenuates right-circularly polarized light (or vice versa) [8]. In this Letter we report on the ability of a columnar thin film (CTF) comprising both dissipative and active component materials to discriminate between incident light of s and p polarization states.

A CTF is an array of parallel identical nanocolumns which may be fabricated by oblique-angle physical-vapor-deposition techniques that include thermal evaporation, electron-beam evaporation, sputtering, and pulsed-laser deposition [9, 10]. Macroscopically, the optical properties of CTFs are equivalent to those of certain orthorhombic crystals. CTFs are attractive platforms for applications such as sensing chemical and biological species [11, 12], due to the ability to engineer their macroscopic optical responses via control over the porosity and the columnar morphology at the fabrication stage.

Consider a CTF with relative permittivity dyadic

$$\underline{\underline{\varepsilon}} = \underline{\underline{S}}_y(\chi) \cdot \underline{\underline{\varepsilon}}_{\text{ref}}^o \cdot \underline{\underline{S}}_y^T(\chi), \quad (1)$$

where the diagonal dyadic

$$\underline{\underline{\varepsilon}}_{\text{ref}}^o = \varepsilon_a \underline{u}_z \underline{u}_z + \varepsilon_b \underline{u}_x \underline{u}_x + \varepsilon_c \underline{u}_y \underline{u}_y, \quad (2)$$

signifies macroscopic orthorhombic symmetry [13], while the rotation dyadic

$$\begin{aligned} \underline{\underline{S}}_y(\chi) = & \underline{u}_y \underline{u}_y + (\underline{u}_x \underline{u}_x + \underline{u}_z \underline{u}_z) \cos \chi \\ & + (\underline{u}_z \underline{u}_x - \underline{u}_x \underline{u}_z) \sin \chi \end{aligned} \quad (3)$$

¹University of Edinburgh, School of Mathematics and Maxwell Institute for Mathematical Sciences, Edinburgh EH9 3FD, UK; Pennsylvania State University, Department of Engineering Science and Mechanics, University Park, PA 16802, USA; email: T.Mackay@ed.ac.uk

²Pennsylvania State University, Department of Engineering Science and Mechanics, University Park, PA 16802, USA

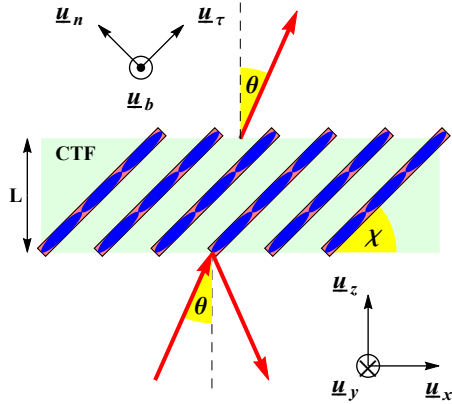


Figure 1: A schematic representation of reflection–transmission for a CTF.

involves the nanocolumn inclination angle $\chi \in (0, \pi/2]$. The unit vectors aligned with the Cartesian axes are represented by the triad $\{\underline{u}_x, \underline{u}_y, \underline{u}_z\}$. The CTF occupies the region between $z = 0$ and $z = L$.

Numerical values for the three relative-permittivity parameters ε_a , ε_b , and ε_c can be estimated using a standard homogenization procedure [10, 14]. To this end, each column of the CTF may be viewed, at the nanoscopic scale, as a collection of highly elongated ellipsoidal inclusions strung together end-to-end, with all inclusions having the same orientation and shape. The dyadic

$$\underline{u}_n \underline{u}_n + \gamma_\tau \underline{u}_\tau \underline{u}_\tau + \gamma_b \underline{u}_b \underline{u}_b \quad (4)$$

specifies the shape of each ellipsoid. Herein the normal, tangential, and binormal basis vectors are specified in terms of the nanocolumn inclination angle χ per

$$\left. \begin{aligned} \underline{u}_n &= -\underline{u}_x \sin \chi + \underline{u}_z \cos \chi \\ \underline{u}_\tau &= \underline{u}_x \cos \chi + \underline{u}_z \sin \chi \\ \underline{u}_b &= -\underline{u}_y \end{aligned} \right\}, \quad (5)$$

whereas $\gamma_b > 0$ and $\gamma_\tau > 0$ are shape factors. The CTF is represented schematically in Fig. 1.

Since the nanocolumnar morphology is highly aciculate, we fixed $\gamma_\tau = 15$ and $\gamma_b = 2$, in keeping with earlier studies [15]. Also the nanocolumns were taken to be made from magnesium monoxide [16] impregnated with about 0.2% v/v silver nanoparticles. Thus, the refractive index of the columnar material was estimated as $1.7310 + 0.0086i$ using the Biot–Arago formula [17], when the free-space wavelength $\lambda_0 = 637$ nm. The void regions of the CTF were supposed to be filled with an active material which is taken to be a mixture of rhodamine 800 and rhodamine 6G. Such a mixture can possess a relative permittivity with imaginary part in the range $(-0.15, -0.02)$ and real part in the range $(1.8, 2.3)$ across the 440–500-THz frequency range, depending upon the relative concentrations and the external pumping rate [2]. We took the relative permittivity of the mixture to be $2 - 0.02i$ for our calculations.

Following the methodology described elsewhere [15], ε_a , ε_b , and ε_c were estimated using the Bruggeman homogenization formalism [18]. These relative permittivity parameters are plotted against porosity $f_v \in (0, 1)$ in Fig. 2. For a narrow range of porosity $f_v \in (0.46, 0.60)$ the imaginary parts of $\varepsilon_{a,b,c}$ have different signs, which indicates that the CTF simultaneously allows attenuation and amplification [6]. For the remainder of this Letter, we set $f_v = 0.53$ at which $\varepsilon_a = 2.4033 - 0.0030i$, $\varepsilon_b = 2.4665 + 0.0032i$, and $\varepsilon_c = 2.43570 + 0.0002i$. Also, the nanocolumn inclination angle was fixed at $\chi = 60^\circ$.

Now we turn to the reflection–transmission problem for the CTF. Suppose that an incident plane wave

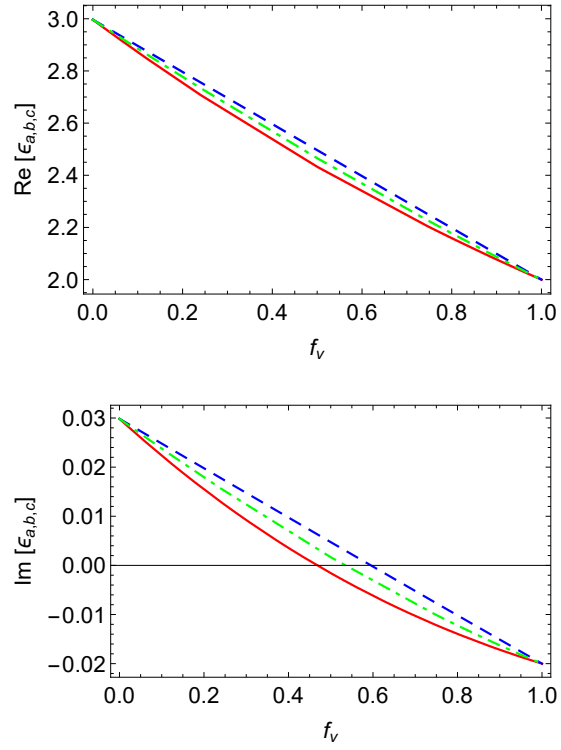


Figure 2: Real and imaginary parts of the relative permittivity parameters ε_a (red solid curves), ε_b (blue dashed curves), and ε_c (green broken dashed curves) plotted against porosity f_v .

exists in the vacuous half-space $z < 0$, as represented by the electric field phasor

$$\begin{aligned} \underline{E}_{\text{inc}} &= \left(a_s \underline{s} + a_p \underline{p}_+ \right) \exp \{ i(2\pi/\lambda_0) \\ &\quad \times [(x \cos \psi + y \sin \psi) \sin \theta + z \cos \theta] \}, \end{aligned} \quad (6)$$

decomposed into s - and p -polarized components, with

$$\left. \begin{aligned} \underline{s} &= -\underline{u}_x \sin \psi + \underline{u}_y \cos \psi \\ \underline{p}_\pm &= \mp (\underline{u}_x \cos \psi + \underline{u}_y \sin \psi) \cos \theta + \underline{u}_z \sin \theta \end{aligned} \right\}. \quad (7)$$

Whereas θ is the angle of incidence with respect to the z axis, ψ is the angle of incidence with respect to the x axis in the xy plane. Correspondingly, the reflected plane wave represented by

$$\begin{aligned} \underline{E}_{\text{ref}} &= \left(r_s \underline{s} + r_p \underline{p}_- \right) \exp \{ i(2\pi/\lambda_0) \\ &\quad \times [(x \cos \psi + y \sin \psi) \sin \theta - z \cos \theta] \} \end{aligned} \quad (8)$$

also exists in the half-space $z < 0$, and the transmitted plane wave represented by

$$\begin{aligned} \underline{E}_{\text{tr}} &= \left(t_s \underline{s} + t_p \underline{p}_+ \right) \exp \{ i(2\pi/\lambda_0) \\ &\quad \times [(x \cos \psi + y \sin \psi) \sin \theta + (z - L) \cos \theta] \} \end{aligned} \quad (9)$$

exists in the vacuous half-space $z > L$.

Following a standard procedure [10], the two reflection amplitudes $r_{s,p}$ and the two transmission amplitudes $t_{s,p}$ may be found in terms of the two incidence amplitudes $a_{s,p}$ per

$$\begin{bmatrix} r_s \\ r_p \end{bmatrix} = \begin{bmatrix} r_{ss} & r_{sp} \\ r_{ps} & r_{pp} \end{bmatrix} \begin{bmatrix} a_s \\ a_p \end{bmatrix} \quad (10)$$

and

$$\begin{bmatrix} t_s \\ t_p \end{bmatrix} = \begin{bmatrix} t_{ss} & t_{sp} \\ t_{ps} & t_{pp} \end{bmatrix} \begin{bmatrix} a_s \\ a_p \end{bmatrix}, \quad (11)$$

wherein the four reflection coefficients $r_{ss,sp,ps,pp}$ and the four transmission coefficients $t_{ss,sp,ps,pp}$ have been introduced. The corresponding reflectances are defined as $R_{sp} = |r_{sp}|^2$ etc., and the corresponding transmittances defined as $T_{ps} = |t_{ps}|^2$ etc.

For a wholly dissipative material (i.e., one that does not simultaneously exhibit attenuation and amplification), it follows from the principle of energy conservation that

$$\left. \begin{aligned} R_{ss} + R_{ps} + T_{ss} + T_{ps} &< 1 \\ R_{pp} + R_{sp} + T_{pp} + T_{sp} &< 1 \end{aligned} \right\}. \quad (12)$$

Similarly, for a wholly active material the inequalities (12) are reversed, i.e.,

$$\left. \begin{aligned} R_{ss} + R_{ps} + T_{ss} + T_{ps} &> 1 \\ R_{pp} + R_{sp} + T_{pp} + T_{sp} &> 1 \end{aligned} \right\}. \quad (13)$$

All eight remittances were computed for $\lambda_0 = 637$ nm. When the azimuthal angle $\psi = 0^\circ$, all four cross-polarized remittances, namely $R_{sp,ps}$ and $T_{sp,ps}$, are null valued. For $\psi = 0^\circ$, the remittance sum $R_{ss} + T_{ss}$ for s -polarized incident light and the remittance sum $R_{pp} + T_{pp}$ for p -polarized incident light are plotted against the polar angle θ for the CTF thicknesses $L \in \{1, 3, 5\}$ μm in Fig. 3. For all values of the polar angle θ , we see that $R_{ss} + T_{ss} < 1$ whereas $R_{pp} + T_{pp} > 1$. Thus, p -polarized incident light is amplified whereas s -polarized incident light is attenuated inside the CTF.

This difference in the responses to s -polarized incident light and p -polarized incident light is generally enhanced as the CTF thickness increases. That is, the degree of amplification for p -polarized incident light

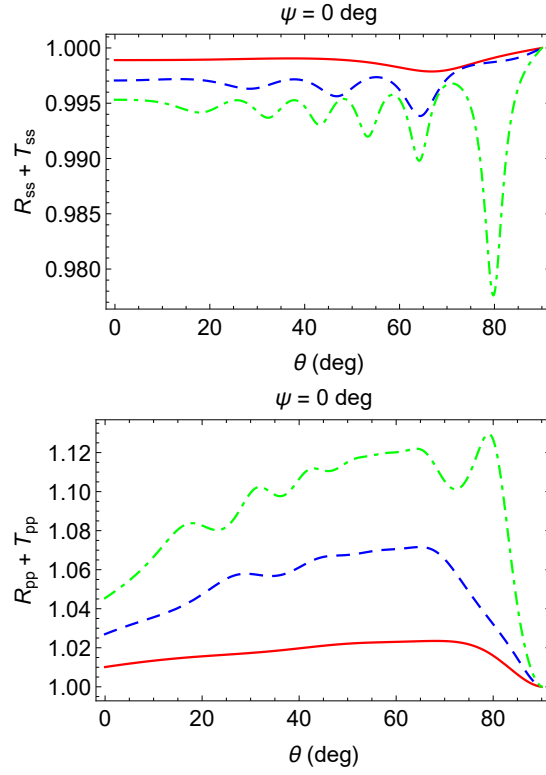


Figure 3: The reflectance–transmittance sums $R_{ss} + T_{ss}$ and $R_{pp} + T_{pp}$ plotted against θ for $\psi = 0^\circ$, when $L = 1 \mu\text{m}$ (red solid curves), $3 \mu\text{m}$ (blue dashed curves), and $5 \mu\text{m}$ (green broken dashed curves).

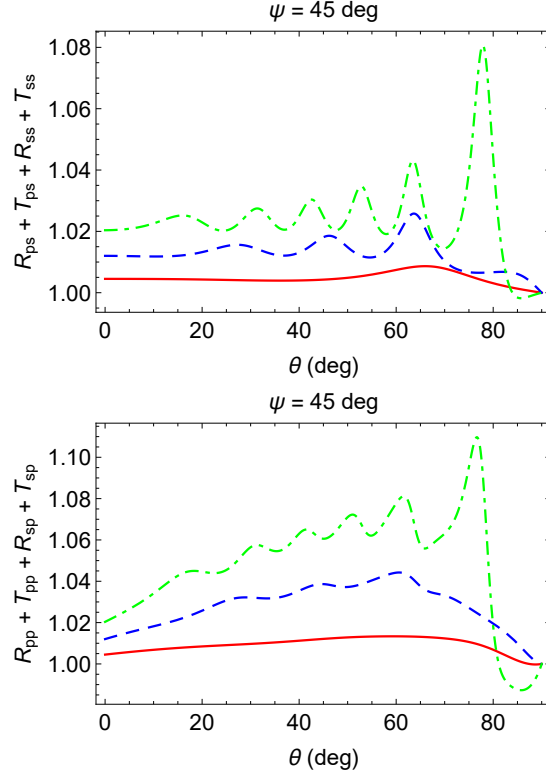


Figure 4: The reflectance–transmittance sums $R_{ss} + R_{ps} + T_{ss} + T_{ps}$ and $R_{pp} + R_{sp} + T_{pp} + T_{sp}$ plotted against θ for $\psi = 45^\circ$, when $L = 1 \mu\text{m}$ (red solid curves), $3 \mu\text{m}$ (blue dashed curves), and $5 \mu\text{m}$ (green broken dashed curves).

is greater for larger values of L and the degree of attenuation for s -polarized incident light is greater for larger values of L .

For $\psi = 45^\circ$, the remittance sum $R_{ss} + R_{ps} + T_{ss} + T_{ps}$ for s -polarized incident light and the remittance sum $R_{pp} + R_{sp} + T_{pp} + T_{sp}$ for p -polarized incident light are plotted against the polar angle θ for thicknesses $L \in \{1, 3, 5\} \mu\text{m}$ in Fig. 4. The picture here is quite different to that for $\psi = 0^\circ$. When $\psi = 45^\circ$ and $\theta < 81^\circ$, the incident light is amplified regardless of its polarization state, and the degree of amplification generally increases as the CTF thickness increases. However, p -polarized incident light is attenuated for $L = 5 \mu\text{m}$ but amplified for smaller values of L when $\theta > 81^\circ$.

Lastly, we turn to the case where $\psi = 90^\circ$, as represented in Fig. 5 wherein the remittance sums $R_{ss} + R_{ps} + T_{ss} + T_{ps}$ and $R_{pp} + R_{sp} + T_{pp} + T_{sp}$ are plotted against θ for $L \in \{1, 3, 5\} \mu\text{m}$. In contrast to what happens for $\psi = 0^\circ$, here s -polarized incident light is generally amplified while p -polarized incident light is generally attenuated. As in Figs. 4 and 5, the degrees of amplification and attenuation are generally exaggerated as the CTF thickness increases. However, there are notable exceptions. For example, for a narrow range of polar angles centered on $\theta = 76^\circ$, p -polarized incident light is amplified for $L = 5 \mu\text{m}$ but attenuated for smaller values of L .

The CTF considered in this Letter represents a practicable proposition, with realistic values being chosen for the relative permittivities of the component materials. By combining a dissipative material for the nanocolumns with an active material to fill the void regions of a CTF, polarization-state-dependent attenuation and amplification may be achieved. Parenthetically, the concept of polarization–state–dependent attenuation and amplification has previously been described for a nonspecific optical system [19]. In contrast, the phenomenon described herein concerns a physically-realizable engineered material. These results open

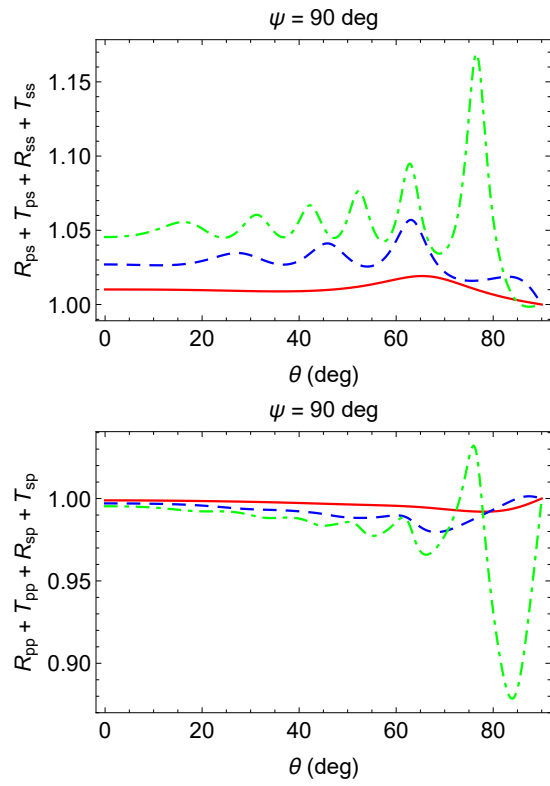


Figure 5: As Fig. 4 except that $\psi = 90^\circ$.

the door for linear polarizers of a new type.

Acknowledgement AL is grateful to the Charles Godfrey Binder Endowment at Penn State for ongoing support of his research.

References

References

- [1] Walser RM 2001 *Proc. SPIE* **4467** 1
- [2] Sun L, Yang X, and Gao J 2013 *Appl. Phys. Lett.* **103** 201109
- [3] Wuestner S, Pusch A, Tsakmakidis K L, Hamm J M, and Hess O 2010 *Phys. Rev. Lett.* **105** 127401
- [4] Dong Z-G, Liu H, Li T, Zhu Z-H, Wang S-M, Cao J-X, Zhu S-N, and Zhang X 2010 *Appl. Phys. Lett.* **96** 044104
- [5] Strangi G, De Luca A, Ravaine S, Ferrie M, and Bartolino R 2011 *Appl. Phys. Lett.* **98** 251912
- [6] Mackay T G and Lakhtakia A 2015 *Phys. Rev. A* **92** 053847
- [7] Cerjan A and Fan A 2017 *Phys. Rev. Lett.* **118** 253902
- [8] Mackay T G and Lakhtakia A 2016 *J. Opt. (UK)* **18** 055104
- [9] Hodgkinson I J and Wu Q h 1997 *Birefringent Thin Films and Polarizing Elements* (Singapore: World Scientific)
- [10] Lakhtakia A and Messier R 2005 *Sculptured Thin Films: Nanoengineered Morphology and Optics* (Bellingham, WA: SPIE Press)
- [11] Lakhtakia A, Messier R, Brett M J, and Robbie K 1996 *Innovat. Mater. Res.* **1** 165–176
- [12] Pursel S M and Horn M W 2007 *J. Vac. Sci. Technol. B* **25** 2611–2615
- [13] Mackay T G and Lakhtakia A 2010 *Electromagnetic Anisotropy and Bianisotropy: A Field Guide* (Singapore: Word Scientific)
- [14] Sherwin J A, Lakhtakia A, and Hodgkinson I J 2002 *Opt. Commun.* **209** 369–375
- [15] Mackay T G and Lakhtakia A 2010 *J. Nanophoton.* **4** 041535
- [16] Stephens R E and Malitson I H 1952 *J. Res. Natl. Bur. Stand.* **49** 249–252
- [17] Biot J-B and Arago F 1806 *Mém. Inst. Fr.* **7** 301–385
- [18] Mackay T G and Lakhtakia A 2015 *Modern Analytical Electromagnetic Homogenization* (Bristol: IOP Publishing)
- [19] Azzam R M A and Bashara N M 1977 *Ellipsometry and Polarized Light* (Amsterdam: North-Holland Publishing)